The International Journal of Advanced Manufacturing Technology (2023) 127:5437–5448
https://doi.org/10.1007/s00170-023-11908-x

ORIGINAL ARTICLE

Submerged arc welding process: a numerical investigation of temperatures, displacements, and residual stresses in ASTM A516-Gr70 corner joined samples

Romina Conte[1] · **David Rodríguez Izquierdo**[1] · **Gagliardi Francesco**[1]

Received: 30 March 2023 / Accepted: 4 July 2023 / Published online: 13 July 2023

Abstract
Arc welding processes represent an important category of fusion welding techniques. They are characterised by the use of an electric arc to create heat to melt and join metals. Submerged arc welding belongs to this process category. Its peculiarities are mainly related to the employment of a continuously fed electrode and of a powdered flux to cover the arc providing electrical conduction between electrode and metals to be connected and, at the same time, generating protective gas and slag shields. Current (I), voltage (V), and welding speed (v) are the main process variables, properly set, to guarantee the specific heat (SH) required to achieve sound weld beads. In this research, finite element models were built looking at the macrographs extracted by experimental tests performed in two steps in order to obtain the real area of each pass and setting different welding conditions. Different combinations of I, V, and v were proposed providing, however, a fixed SH to the welding zone according to the required industrial standards. Specifically, tests were executed increasing the ratio V to v (for a constant I) and the ratio I to v (for a constant V) and with a different combination of V and I maintaining constant their product (for a constant v). The influence of the investigated variables' combination on the weld pool in terms of depth and width was discussed. Finally, the validated numerical models were employed to highlight precisely residual stresses and displacements trend on cross-sectioned weld beads connecting the shown tendencies to the investigated process conditions.

Keywords Submerged arc welding · Numerical analysis · Corner joint · Temperature phases · Stress · Displacement

1 Introduction

Fusion welding allows two base materials to be joined by heating them to the melting point with or without pressure setting and/or filler materials. When the welding is performed, heating and cooling phases are very rapid. A thermal cycle is, therefore, executed affecting the grain structure of the processed materials close to the welding line. This means that a new metallurgical condition is created inside an area defined as heat affected zone (HAZ) [1, 2].

Different fusion welding techniques exist and they are widely diffused in the industrial sector. Nevertheless, not all welding approaches have a universal application owing to some specific characteristics/requirements. Among all the existing techniques, the arc welding processes produce coalescence of metals by heating them with an arc between an electrode and the workpiece. The first applied arc welding process was the carbon arc welding (CAW) [3] followed soon by others, such as shielded metal arc welding (SMAW) [4], gas tungsten arc welding (GTAW) [5], gas metal arc welding (GMAW) [6], and submerged arc welding (SAW) [7]. They differ from each other for the typology of electrodes used to generate the arc [1].

This study focuses on SAW, which is characterised by the highest efficiency considering the energy used to initiate the arc [8–10]. SAW allows workpieces made of carbon steel, stainless steel, cast iron, and nickel alloys to be welded, while it is not suitable when titanium or copper alloys are involved in the joint. This welding technique is mostly used when pressure vessels, bridges, and, generally, large structures have to be constructed [11]. In SAW, the arc is generated by a metal electrode which acts as filler material. A granular flux is deposited simultaneously on

✉ Romina Conte
romina.conte@unical.it

[1] Department of Mechanical, Energy and Management Engineering, University of Calabria, Ponte P. Bucci Cubo 45/C, Arcavacata di Rende, CS 87036, Italy

the workpiece by a feed hopper in order to (i) add alloying elements, (ii) create an environment for initiating the arc which remains not visible and stable, during the whole process, and (iii) protect the welded surface from external agents and atmospheric contaminants by means of generated gases. This granular flux, released during the process, is not completely consumed. In fact, just a part is melted, becoming slag after solidification on the weld. This slag needs to be removed before starting a second welding step. The remaining part may be, instead, recovered or recycled, according to the flux typology.

The soundness of the performed welding procedure depends on the process variables to be set. Specifically, the electrode diameter, the current (I), the voltage (V), and the welding speed (v) are the main variables to be taken into account [7, 12–14]. Jou [15] highlighted the importance of the weld bead geometry on the mechanical properties of the weld itself. Experimental tests have been carried out to find out the correlation between current, voltage, welding speed, arc length, and the obtained weld bead. The attention was mainly focused on the effect of the arc length on the heating magnitude. Furthermore, the SAW process has been investigated by numerical analyses since the 1970s. At the beginning, the aim was to predict the thermal and mechanical behaviour of the material by using simplified 2D models, mostly due to the computational limitations and to reduce the overall computing time. During the years, advanced mathematical languages have been developed and the calculation capacity has been improved, too [16]. Nevertheless, according to the scientific literature review, many researchers still prefer modelling in 2D, using flat and asymmetric models, and setting hypotheses and simplifications [17, 18]. Three-dimensional maps, reproducing the thermo-mechanical behaviour of welds, have been, however, always more simulated [16, 19]. Romaní et al. [20] formulated a finite element model by Abaqus for investigating the influence of some welding parameters. The results were compared with the measurements obtained from several coupons. After this preliminary study, a three-dimensional model was developed to understand how the variables affect the thermal cycles, deformations, and residual stresses. Ramos et al. [21] reported the results of a numerical analysis, specifying the main factors to be considered during the model construction. More in detail, the authors first measured the extension of the fused and of the heated affected zone and then the grain size, as well as the hardness profile. The implemented numerical model allowed them to simulate the welding and cooling conditions, demonstrating the congruence between numerical and experimental results.

In the research presented herein, a commercial finite element code was employed aiming at understanding the influence of the main working parameters on the thermal and mechanical properties of a corned welded joint executed by a multi-pass process. The procedure for the model construction was presented and discussed. Several working conditions were simulated setting the numerical simulations starting from experiments executed for each selected process configuration. The numerical study was carried out highlighting how the changing of specific process variables, i.e. I, V, and v, affects the performance of the parts focusing the attention on distortions and residual stresses in the simulated weld beads.

2 Experiments, numerical model and applied method

2.1 Experimental tests

A scheme of SAW process is reported in Fig. 1. The experiments were performed on a power wave AC/DC 1000 SD machine. The processed base material is an ASTM A516 grade 70 [22]. It is a medium carbon alloy, which contains other elements such sulphur, manganese, silicon, and phosphorus. The choice was related to the wide employment in several industries to manufacture, for example, welded pressure vessels, heat exchanges, structural tubing, automotive parts.

As concerns the continuous electrode wire, a copper-coated wire, named AWS A5.17 electrode, was used. It is characterised by a high manganese content. The compositions of the base material and of the electrode are reported in Table 1.

Furthermore, a low manganese and silicon content granular welding flux was selected (https://esab.com/ss/mea_en/products-solutions/product/filler-metals/submerged-arc-wires-and-fluxes-saw/mild-steel-low-alloy-fluxes/ok-flux-10-61/), according to the wire, and employed to protect and enrich the welded surface.

2.2 Numerical model

To the specific aim of this study, the commercial software ESI SYSWELD was used for the numerical investigation which was carried out by considering the experimental tests, effectively performed. The definition of the numerical model starts by analysing the heat source, which size and shape strongly affect the temperature trend within the welded part [23]. The heat source was represented as a double ellipsoid in movement, as proposed by Goldak [24, 25]. Specifically, a three-dimensional Goldak's double-ellipsoid was modelled considering five parameters which are (i) the arc efficiency η, (ii) half width of the fused zone a, (iii) its penetration depth b, (iv) its front length c_f, and (v) its back length c_b (Fig. 2). The experimental data are fundamental in calibrating the heat source. Indeed, a trial-and-error approach was adopted,

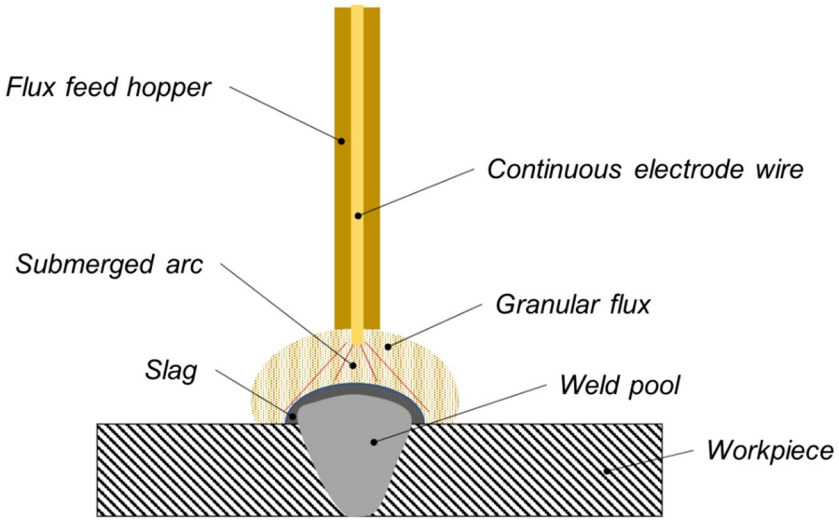

Fig. 1 Sketch of the SAW process

Table 1 Chemical composition of ASTM A516 grade 70 and of AWS A5.17

	C [%]	Mn [%]	P [%]	S [%]	Si [%]	Cu [%]
ASTM A516	0.31	1.2	0.035	0.035	0.45	-
AWS A5.17	0.10	1.8	0.019	0.013	0.05	0.05

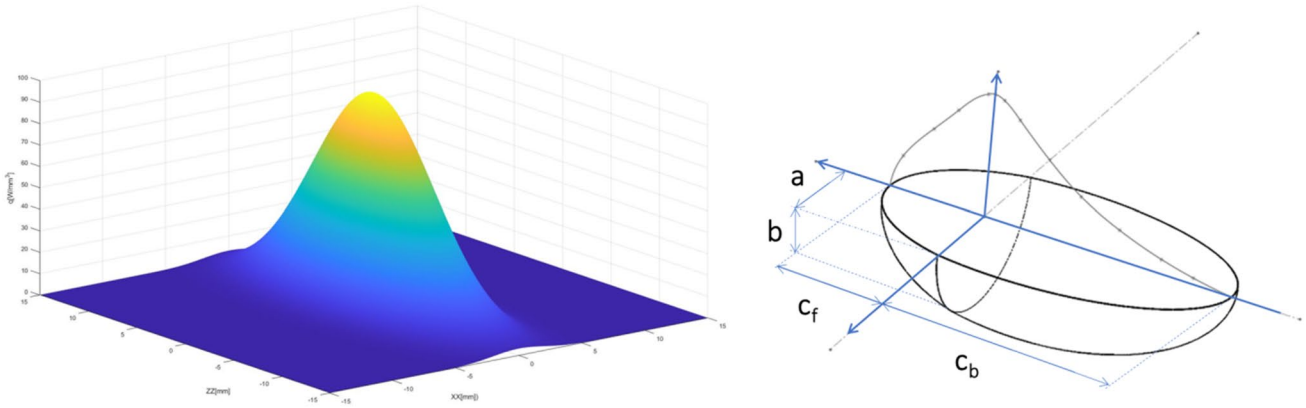

Fig. 2 Goldak's double-ellipsoid and parameters

by comparing the temperature distribution obtained numerically and the weld bead observed experimentally. The details of the numerical and experimental tests are reported in Section 2.3. The values of Goldak's parameters were accurately calibrated by comparing the numerical temperature tendency with the HAZ observable from the macrographs extracted by optical microscopic analyses on each related sample after the required surface treatments. This is a fundamental step to achieve numerical results as accurate as possible.

The properties of the material components, both base and filler material, are chosen from the database already available in the SYSWELD library, following the compositions highlighted in Table 1.

2.3 Methods

Blanks of two different thicknesses, specifically 10 mm and 25 mm (Fig. 3a), were selected to be joined in order to analyse the welding conditions of a typical corner joint. The red part in Fig. 3b displays the blank parts fixed in x, y, and z. To this aim the clamping system shown in Fig. 3c was designed and used for the tests.

An example of the macrograph of one of the sectioned samples is reported in Fig. 4.

It is worth pointing out that since the multi-pass corner joint was performed by following a usual procedure applied in industries, three different welding phases were executed

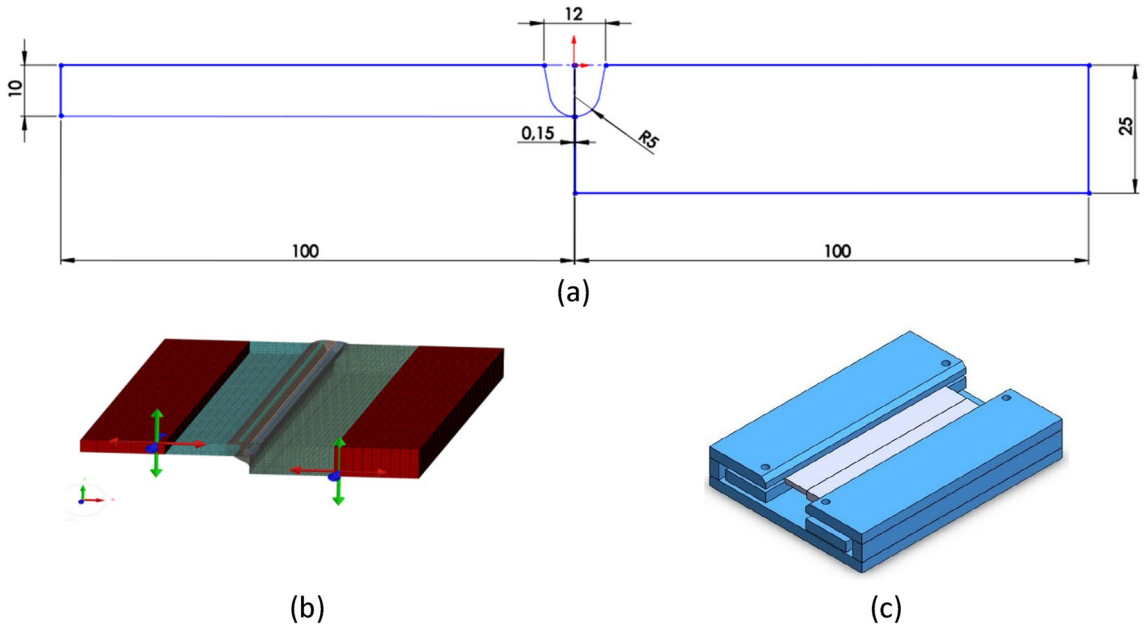

Fig. 3 **a** Coupon geometry, **b** numerical, and **c** experimental clamping system

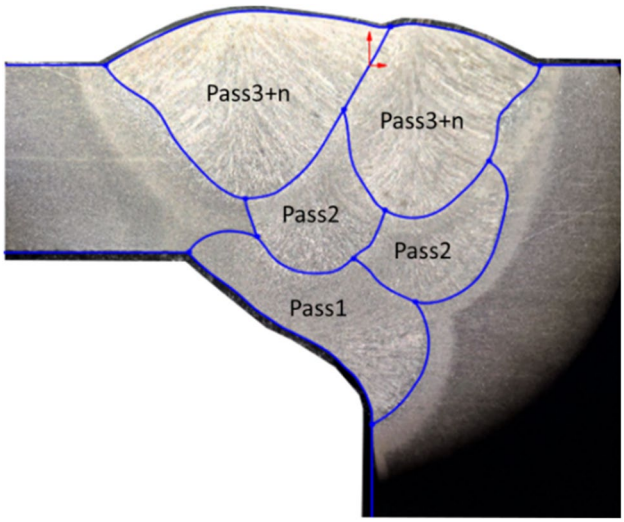

Fig. 4 Geometry of a sectioned weld bead at the end of the process

(Fig. 4): *Pass 1* performed on the downside of the plates to achieve a weld cup between the blanks previously caulked and *pass 2* and *pass 3* + *n* performed both on the upside of the plates with different process parameters to avoid the breach of the weld cup during *pass 2*. *Pass 2* was performed twice moving on the left and on the right side with respect to the centreline of the weld bead. After that, the same procedure was repeated for *pass 3*. For the chosen configuration, a sequence of two *pass 3* was required to fill the weald bead up.

To set the simulations properly, the precise geometries of the weld bead have to be extracted after that each welding sequence is completed. Therefore, the geometries derived from *pass 2* have to be extracted by the experiments before running the *pass 3* phases, which inevitably modify the shape of the previously formed weld bead. For this reason, each process configuration was repeated twice because just *pass 2* was performed on one of the samples, for each case, before its sectioning to extract the macrograph of the weld bead Fig. 5a. Figure 5b and c show an example of a 2D meshed section employed in the numerical analyses of the *pass 2* and *pass 3* phases, respectively. A 3D model of the weld bead at phase 3 is displayed in Fig. 5d.

The discretisation of the welded joint was carried out in order to guarantee a great regularity of the elements, considering orthogonality between the edges with the nodes. A control of the density of the mesh was used, choosing linear quadrilateral elements combined in some areas with triangular elements. The mesh was built finer close to the weld zone and to the heat affected zone and progressively increased moving to the unaffected area. At the end, each configuration was discretised by a customised number of 3D elements (Table 2) due to the specificity of each weld bead.

Each welding pass was launched in the experimental tests, monitoring the temperature on the specimen, once the temperature on the sample surface drops under 250 °C. The idle times between the consecutive phases were recorded and utilised in setting the numerical models. Indeed, the moving heat source module of ESI SYSWELD was employed to simulate the transient process conditions.

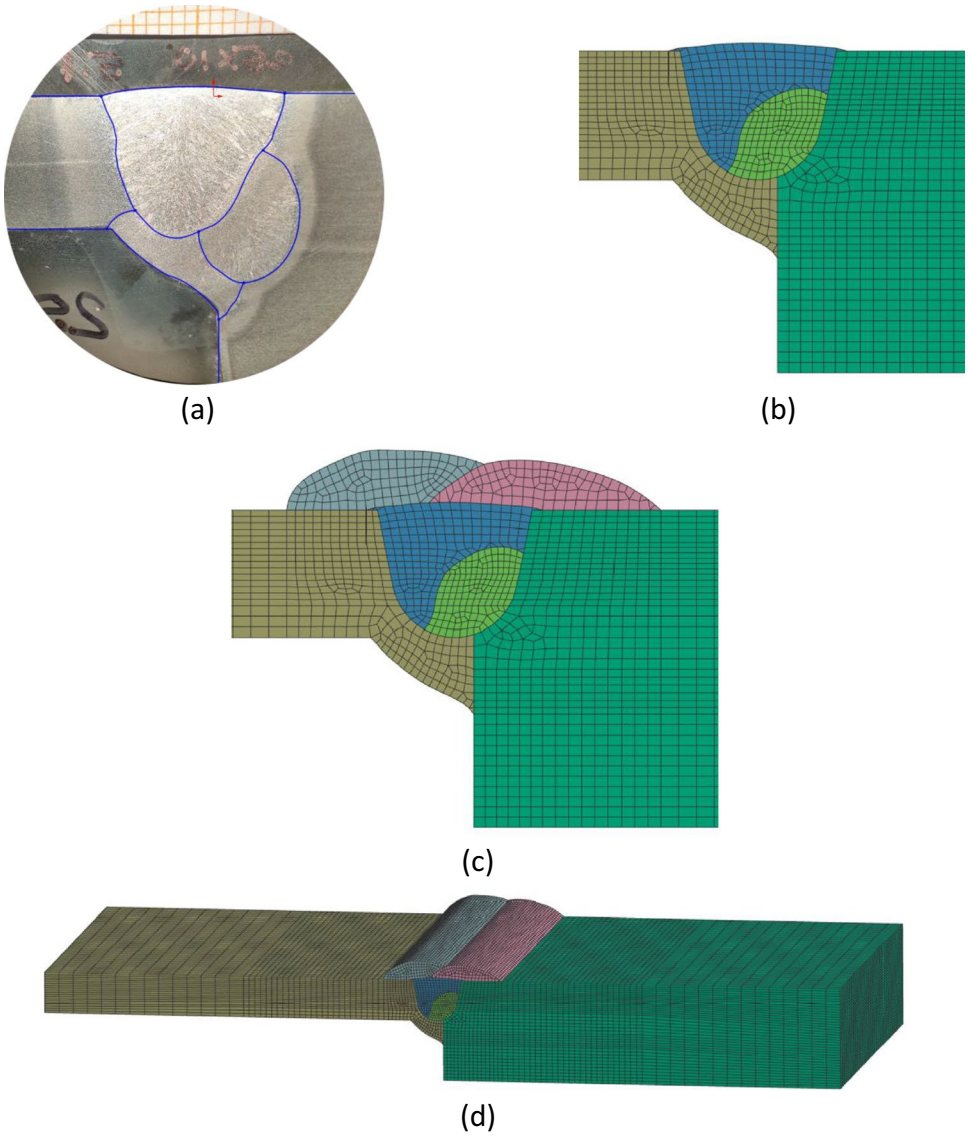

Fig. 5 **a** Macrograph of the weld bead at the end of pass 2, **b** the related 2D meshed section, **c** 2D mesh of the completed pass 3 phases, and **d** and the derived 3D model employed in the numerical analysis

Table 2 Number of 3D element for each test

	# Test				
	Test 1	Test 2	Test 3	Test 4	Test 5
# 3D elements	47,350	179,300	100,950	55,200	64,600

Table 3 SAW process parameters for pass 1 of the welding phase

# Test	Current *I* [A]	Voltage *V* [V]	Welding speed *v* [mm/min]
All tests	440	27	320

Table 4 SAW process parameters for Pass 2 of the welding phase

# Test	Current *I* [A]	Voltage *V* [V]	Welding speed *v* [mm/min]
Test 1	404	34	384
Test 2	540	25,4	384
Test 3	471	34	448
Test 4	540	29,7	448
Test 5	605	34	576

The process parameters set for each pass are the current (I), the voltage (V), and the welding speed (v). The values used for each phase are listed in Tables 3, 4, and 5. The values were chosen to perform the welding following specific heat inputs that were maintained constant for each configuration in order to respect the UNI EN ISO 3834 quality standards. The tests were modified by changing the *pass 2* parameters and fixing the values of the other two phases. Five different process configurations were tested. The values

of the selected parameters were not spaced proportionally because the chosen ranges were driven by the characteristics of the power wave AC/DC 1000 SD machine employed to execute the experiments.

3 Discussion of the results

The macrograph images of the five experimental weld beads, sectioned and etched, and the related predicted numerical temperatures, reporting the maximum reached values in each element during the all analysed process phases, are reported in Figs. 6, 7, 8, 9, and 10. The melting temperature is the upper set value of the scale (1600 °C) in Figs. 6, 7, 8, 9, and 10b) in order to be able to observe the predicted melted areas allowing a comparison between experiments and numerical results. Furthermore, the lower value of this scale (700 °C) is related to the beginning of the steel austenite transition zone to be able to show the heat affected zones (HAZ). Therefore, the shape of the Goldak's double ellipsoid and the precise positions of the heat source for each pass of the performed welding sequences were calibrated and defined to achieve a relevant similarity between macrograph images (Figs. 6, 7, 8, 9, and 10a) and numerical temperature trends (Figs. 6, 7, 8, 9, and 10b), looking at both melted and heat affected zones. More in detail, the continuous line identifies the welding zone, while the heat affected zone is indicated by the dash-dot line.

Table 5 SAW process parameters for Pass 3 of the welding phase

# Test	Current I [A]	Voltage V [V]	Welding speed v [mm/min]
All tests	675	34	768

The optimised numerical simulations were employed to analyse the influence of the investigated process parameters on the temperature trend in the area of the weald bead. As highlighted in Section 2.3, the different process sequences were changed modifying I, V, and v of *pass 2* proportionally to guarantee a constant specific heat for each investigated process configuration. Comparing Figs. 6 and 7 or Figs. 8 and 9, the influence of changing I and V at constant v can be observed. Specifically, if the required specific heat is produced by increasing I to the detriment of V, a deeper weld bead is obtained as a result of a hotter weld pool. Looking at the weld bead's core, the zones that are processed with a higher V in *pass 2* phases, i.e. tests 1 and 3, are, instead, characterised by a slightly wider area. The influence of v increment can be instead watched comparing tests 1, 3, and 5 at V constant and tests 2 and 4 at I constant. In detail, looking at the tests performed with a constant ratio I to v, the heat lost by conduction is strictly related to the process time. Therefore, even if the same specific heat was given to the plates, the weld bead progressively becomes deeper at increasing velocity. For the fastest configuration, test 5, the pass 2 phases affect the bottom part of the weld cup more considerably, reaching a maximum predicted temperature of around 1200 °C. This effect of the velocity is not evident if the welding process is performed at constant I and with a constant ratio V to v (see test 2 and test 4). Indeed, for this

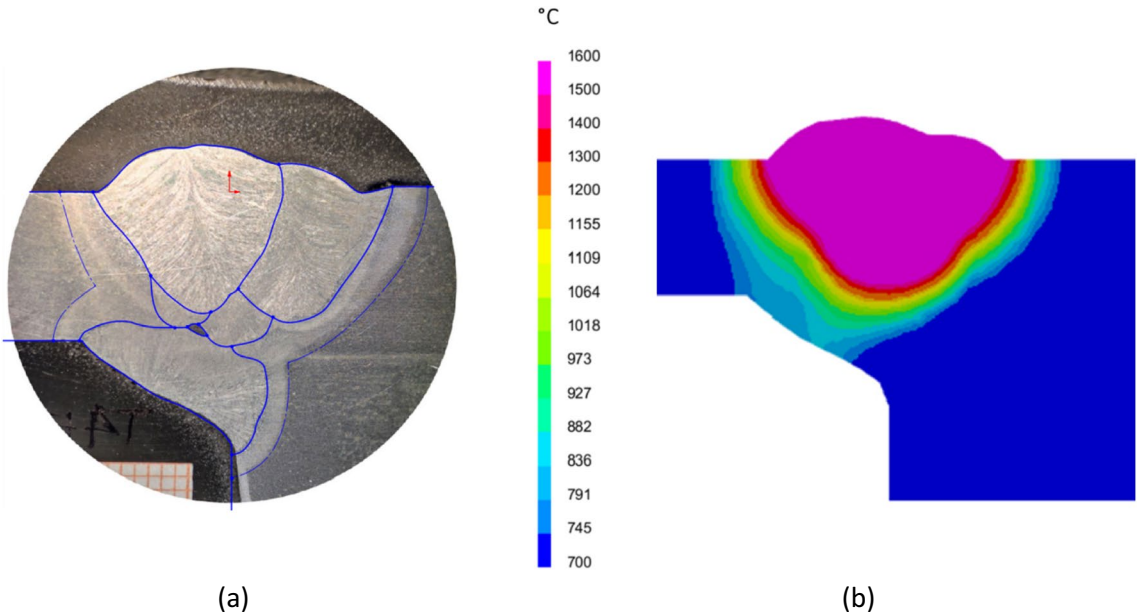

Fig. 6 **a** Macrograph image at the end of the joining process and **b** the numerically extracted maximum temperature trend in each part of the weld bead (test 1)

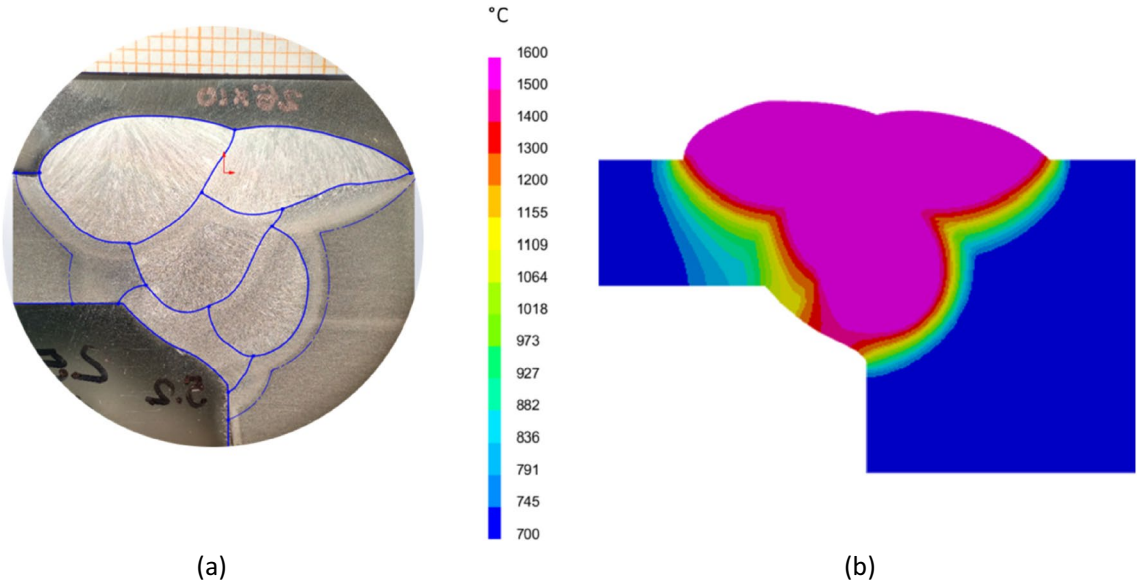

Fig. 7 **a** Macrograph image at the end of the joining process and **b** the numerically extracted maximum temperature trend in each part of the weld bead (test 2)

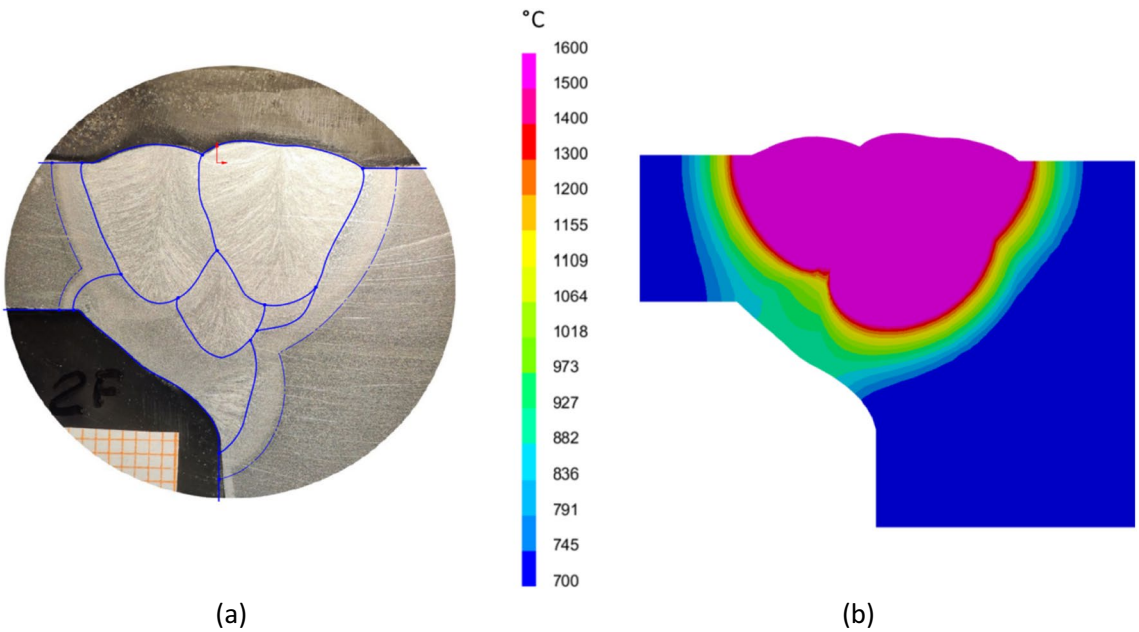

Fig. 8 **a** Macrograph image at the end of the joining process and **b** the numerically extracted maximum temperature trend in each part of the weld bead (test 3)

case, the conditions were close to melt the weld cup on the downside of the plates to be joined for the slowest v. This evidence is ascribable to the effect of V, whose increment results as prevalent in lowering the penetration of the material's hot bath and in its widening.

The optimised numerical simulations were, moreover, employed in analysing the effects of the highlighted SAW variables in terms of residual stress and displacements on the weld beads at the end of the process. Specifically, the welding speed affects the residual stress considerably. More in detail, Fig. 11 displays the longitudinal tensions generated in the cross-sectional central area of the welded joint. The process configurations, which show a less loaded area of the weld bead, are the ones related to the slowest tested v values. A v increment results in a progressive enhancement of the predicted residual stress if this increment is combined

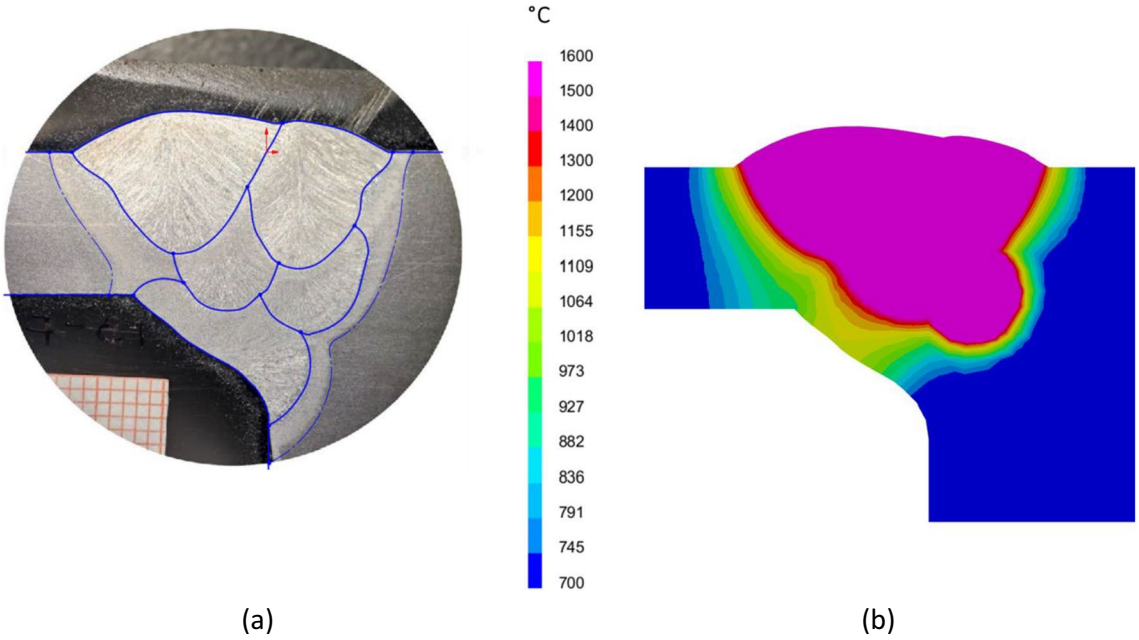

Fig. 9 **a** Macrograph image at the end of the joining process and **b** the numerically extracted maximum temperature trend in each part of the weld bead (test 4)

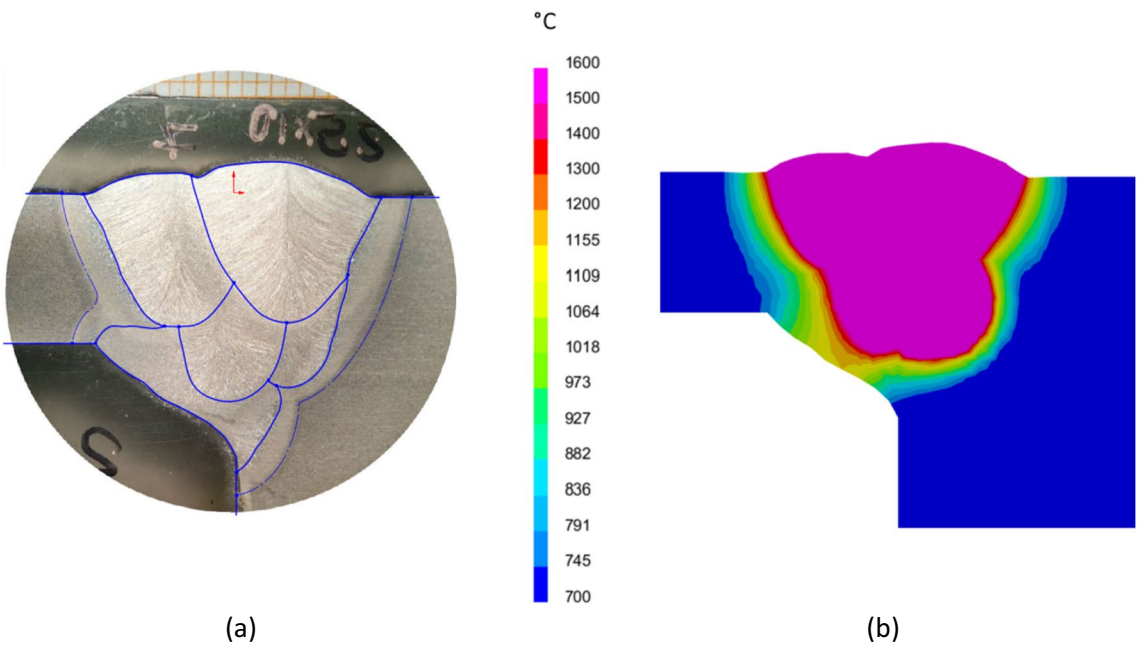

Fig. 10 **a** Macrograph image at the end of the joining process and **b** the numerically extracted maximum temperature trend in each part of the weld bead (test 5)

to the change of I to respect the specific heat constancy (see the residual stress of test 1, test 3, and test 5). This effect is ascribable to a more sudden temperature variation that contributes to a more severe thermal cycle the material is subjected to. The increment of V, instead, producing a wider and outward heat distribution, mitigates the effects of the temperature gradients (see the residual stress of test 2 and test 4). The last facts can be further validated comparing the numerical trends extracted by test 1 and test 2 or test 3 and test 4, where the opposite impact of I and V results in a not

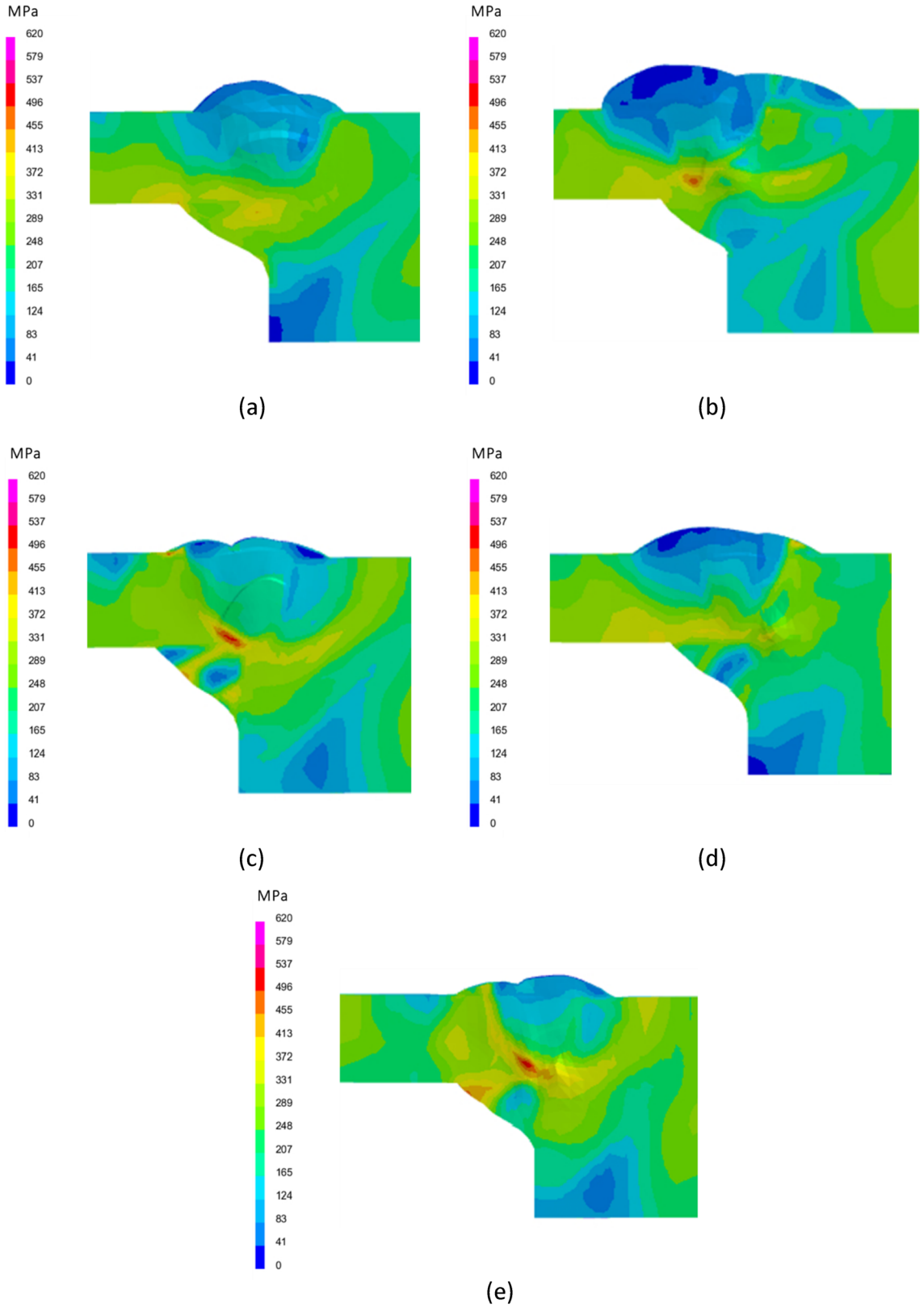

Fig. 11 Numerical trend of the residual stresses on the weald bead for **a** test 1, **b** test 2, **c** test 3, **d** test 4, and **e** test 5

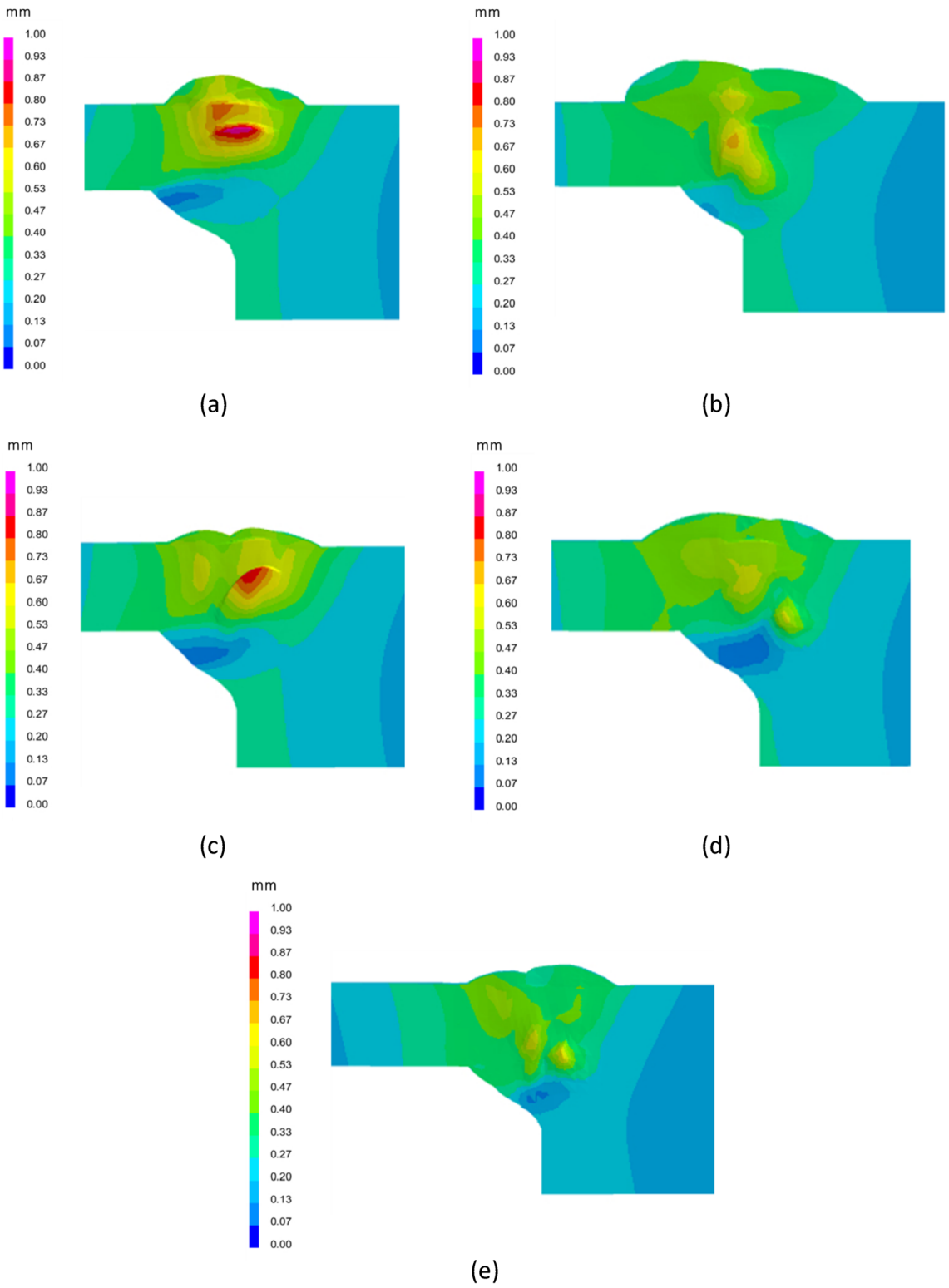

Fig. 12 Numerical trend of the weald bead's displacement for **a** test 1, **b** test 2, **c** test 3, **d** test 4, and **e** test 5

marked and consistent residual stress variation for process configurations characterised by constant welding speeds.

The welding speed on the displacement trend shows an opposite effect with respect to the residual stresses with its influence that is more pronounced at decreasing of v and at increasing of V at detriment of I (Fig. 12). Indeed, considering just the v influence, the zone of the weald bead interested in a significant temperature variation is wider owing to more

time available to dissipate heat by conduction. The thermal expansion, therefore, concerns part of the material closer to the clamping zone affecting also the displacement of the welding bead area. Same considerations can be deduced taking into account the influence of I and V. Indeed, the increment of V to the detriment of I leads to an influence of the welding phase more spread up to the plate width with respect to its thickness with the displacements that go through quite a more relevant variation at voltage enhancement. The discussed results can be observed comparing the same tests pointed out for the residual stress argumentation.

4 Conclusion

The steps for setting a numerical model, employable for the analysis of multi-pass welding process, were highlighted. Specifically, macrograph images of weld beads obtained by experiments were utilised to calibrate the heat source and to define its position during the welding passes overlapping the melted and the heat affected areas and the temperature distribution of the weald bead for each analysed process configuration. Indeed, the main welding variables, i.e. current, voltage, and welding speed, were combined to guarantee a constant specific heat input with respect to the UNI EN ISO 3834 standards and according to the characteristics of the employed welding machine. The influences of each analysed variable on the weld bead shape were pointed out postprocessing the optimised models. The results deduced by the numerical observations confirm what is already known in literature on I, V, and v. In addition to that, the specific analysed conditions highlighted that deeper weld beads are obtained preferring an increment of I to the detriment of V or to an increment of v, maintaining constant the specific input heat during the process. The increment of V, instead, results to be relevant in lowering the penetration of the material's hot bath and in its widening. Furthermore, the strength of the proposed numerical models has to be ascribed to the possibility of evaluating main outputs for judging the welding performance, such as residual stress on the weld bead and displacement of the joined parts, looking at the weld bead area, locally. The evaluation of these outputs results would be complex, expensive, and time consuming if experimentally performed. More in detail, V and I, analysed in a perspective of a restricted variation, result in lowering the displacements at increment of I and a decrement of V while the residual stresses show a not consistent trend for an opposite influence of these variables. The V randomness for the residual stress distribution is further confirmed considering that a v increment, only if combined to the I variation, entails an increasing of predicted residual stress. At the same time, a decrement of displacement is always observable at V reduction for specific heat process constancy.

The extracted numerical evidence in terms of residual stresses and displacements, even though justifiable by the performed remarks, needs experiments to be validated. This step will be the natural development, which the activities of this research are moving to.

Author contribution All authors contributed to the study conception and design. Experimental test, data collection, and analysis were performed by all authors. The authors contributed in writing the first draft and they commented on previous versions of the manuscript. All authors read and approved the final manuscript.

Funding Open access funding provided by Università della Calabria within the CRUI-CARE Agreement.

Declarations

Competing interests The authors declare no competing interests.

References

1. Zhang M, Han Y, Jia C et al (2022) Improving the microstructures and mechanical properties with nano-Al2O3 treated wire in underwater submerged arc welding. J Manuf Process 74:40–51. https://doi.org/10.1016/j.jmapro.2021.11.056
2. Datta S, Bandyopadhyay A, Pal PK (2008) Application of Taguchi philosophy for parametric optimization of bead geometry and HAZ width in submerged arc welding using a mixture of fresh flux and fused flux. Int J Adv Manuf Technol 36:689–698. https://doi.org/10.1007/s00170-006-0894-7
3. Lincoln JC (1930) Electric welding by the carbon arc. J AIEE 49:110–113. https://doi.org/10.1109/JAIEE.1930.6534877
4. Pathak D, Pratap SR, Gaur S et al (2021) To study the influence of process parameters on weld bead geometry in shielded metal arc welding. Mater Today Proc 44:39–44. https://doi.org/10.1016/j.matpr.2020.06.164
5. Giridharan PK, Murugan N (2009) Optimization of pulsed GTA welding process parameters for the welding of AISI 304L stainless steel sheets. Int J Adv Manuf Technol 40:478–489. https://doi.org/10.1007/s00170-008-1373-0
6. Kiran DV, Cheon J, Arif N et al (2016) Three-dimensional finite element modeling of pulsed AC gas metal arc welding process. Int J Adv Manuf Technol 86:1453–1474. https://doi.org/10.1007/s00170-015-8297-2
7. Houldcroft PT (1989) Submerged-arc welding. Abington Publishing Woodhead

8. Singh R (2020) Applied welding engineering: processes, codes, and standards. Butterworth-Heinemann
9. Murugan N, Parmar RS, Sud SK (1993) Effect of submerged arc process variables on dilution and bead geometry in single wire surfacing. J Mater Process Technol 37:767–780. https://doi.org/10.1016/0924-0136(93)90135-S
10. Rao RV, Kalyankar VD (2013) Experimental investigation on submerged arc welding of Cr–Mo–V steel. Int J Adv Manuf Technol 69:93–106. https://doi.org/10.1007/s00170-013-5007-9
11. Edwin Raja Dhas J, Anton Savio Lewise K, Laxmi G (2022) Submerged arc welding process parameter prediction using predictive modeling techniques. Mater Today Proc 64:402–409. https://doi.org/10.1016/j.matpr.2022.04.757
12. Aswal VK, Jain JK, Sonia P (2021) Review on the behavior of various parameters on heat distribution in the SAW process. Mater Today Proc 47:6734–6739. https://doi.org/10.1016/j.matpr.2021.05.123
13. Vedrtnam A, Singh G, Kumar A (2018) Optimizing submerged arc welding using response surface methodology, regression analysis, and genetic algorithm. Def Technol 14:204–212. https://doi.org/10.1016/j.dt.2018.01.008
14. Choudhary A, Kumar M, Unune DR (2019) Experimental investigation and optimization of weld bead characteristics during submerged arc welding of AISI 1023 steel. Def Technol 15:72–82. https://doi.org/10.1016/j.dt.2018.08.004
15. Jou M (2001) Experimental investigation of resistance spot welding for sheet metals used in automotive industry. JSME Int J Ser C 44:544–552. https://doi.org/10.1299/jsmec.44.544
16. Miller DK (1999) What every engineer should know about welding procedures. Weld J 78(8):37–43
17. Quinn TP, Szanto M, Gilad I, Shai I (2005) Coupled arc and droplet model of GMAW. Sci Technol Weld Join 10:113–119. https://doi.org/10.1179/174329305X29492
18. Cortés PR, Villanueva AJ, Ponce E et al (2004) Estudio de la soldabilidad y corrosión del acero inoxidable AISI 904L con los agentes utilizados en la lixiviación del cobre. Rev Fac Ing - Univ Tarapacá 12(2):43–56. https://doi.org/10.4067/S0718-13372004000200007
19. Nezamdost MR, Esfahani MRN, Hashemi SH et al (2016) Investigation of temperature and residual stresses field of submerged arc welding by finite element method and experiments. Int J Adv Manuf Technol 87:615–624. https://doi.org/10.1007/s00170-016-8509-4
20. Romaní G, Portolés A (2008) Modelo tridimensional de simulación por MEF para estudiar la influencia de variables esenciales de soldadura robotizada GMAW en uniones a tope planas. In: Soldadura y tecnologías de unión 19(109):22–26
21. Ramos HME, Tavares SMO, de Castro PMST (2018) Numerical modelling of welded T-joint configurations using SYSWELD. Sci Technol Mater 30:6–15. https://doi.org/10.1016/j.stmat.2018.08.002
22. Ali A, Sanuddin A (2009) Characterization of ASTM A516 grade 70 fusion welded joints. Int Rev Mech Eng 3(5)
23. Sharma A, Chaudhary AK, Arora N, Mishra BK (2009) Estimation of heat source model parameters for twin-wire submerged arc welding. Int J Adv Manuf Technol 45:1096–1103. https://doi.org/10.1007/s00170-009-2046-3
24. Goldak J, Chakravarti A, Bibby M (1984) A new finite element model for welding heat sources. Metall Trans B 15:299–305. https://doi.org/10.1007/BF02667333
25. Chujutalli JH, Lourenço MI, Estefen SF (2020) Experimental-based methodology for the double ellipsoidal heat source parameters in welding simulations. Mar Syst Ocean Technol 15:110–123. https://doi.org/10.1007/s40868-020-00074-4